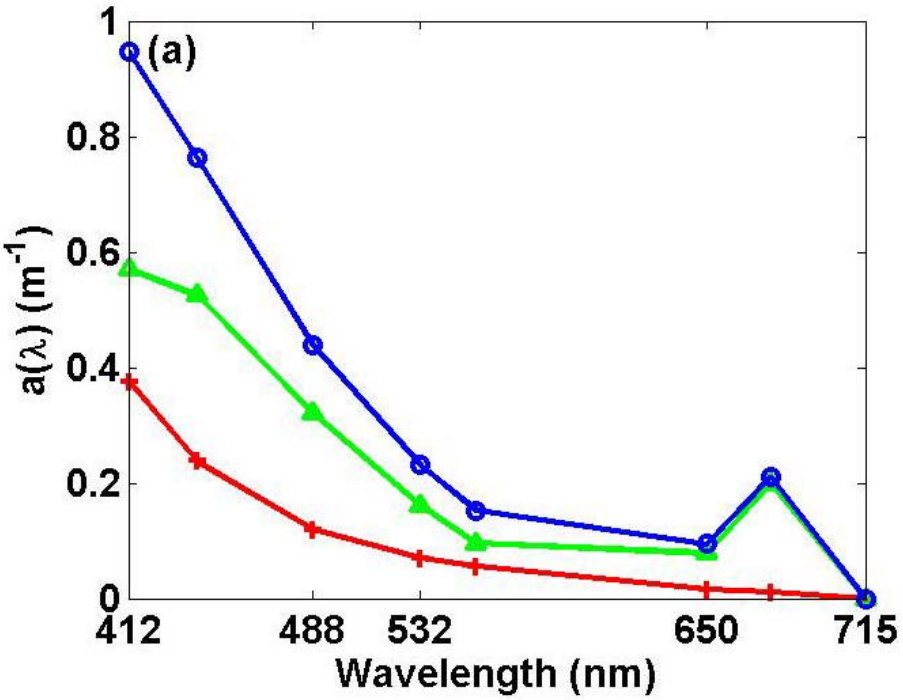

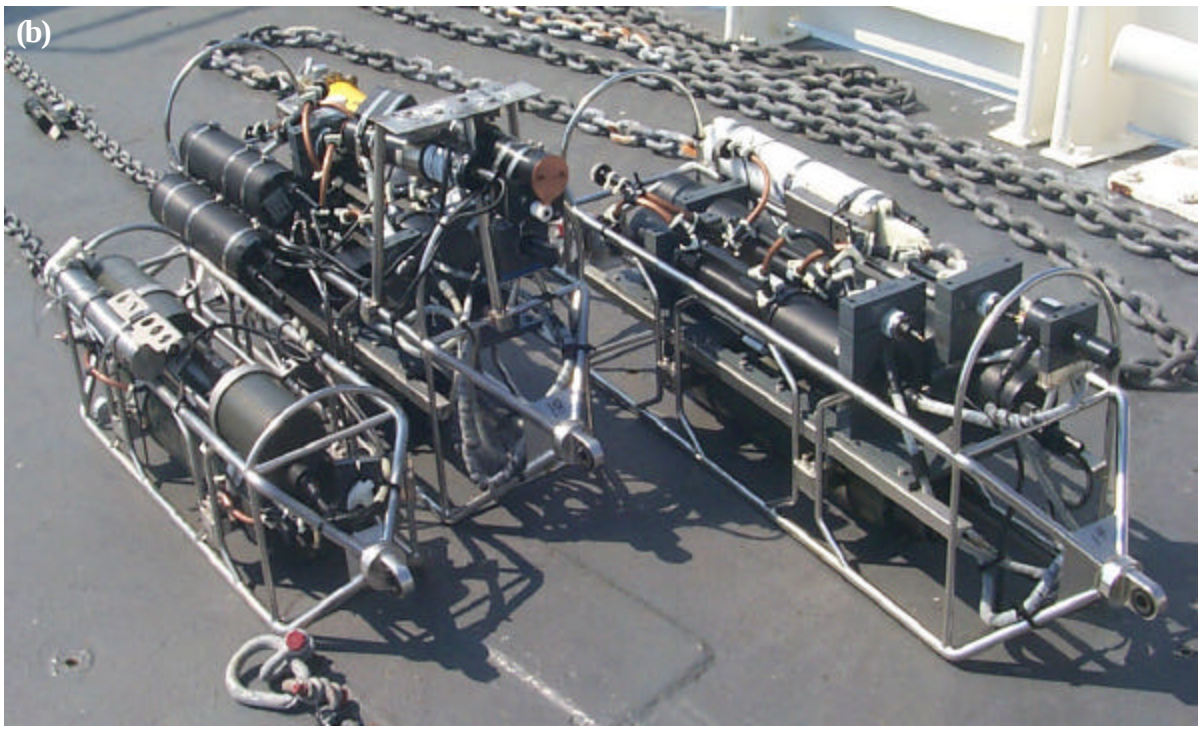

Fig. 1. (a) Example of upper water column absorption spectra (nine wavelengths) for total minus water ($a_{t\text{-}w;}$ circles), particulate ($a_{p;}$ triangles), and gelbstoff ($a_{g;}$ crosses) measured at the LEO-15 site (5 km offshore, 15 m water depth). Note $a_p = a_{ph} + a_d$. (b) Photograph of moored bio-optical systems used to measure inherent and apparent optical properties: nine-wavelength spectral absorption-attenuation, beam c, PAR, upwelling radiance, downwelling irradiance, and chlorophyll fluorescence.

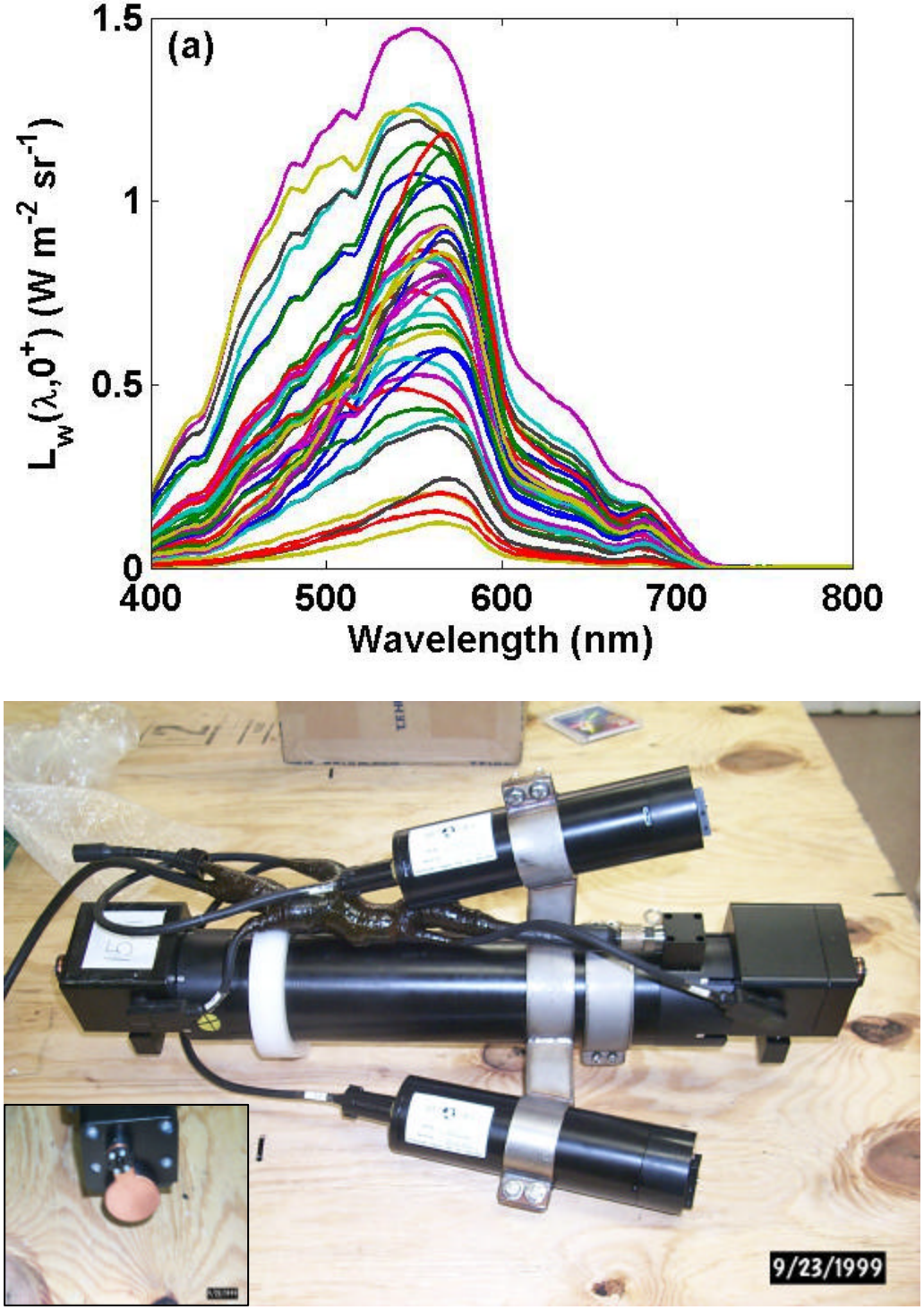

Fig. 2. (a) Example of water-leaving radiance spectra derived from radiometric measurements collected at the LEO-15 site (25 km offshore, 24 m water depth). (b) Photograph of an optical system used to measure inherent and apparent optical properties: upwelling radiance and downwelling irradiance, chlorophyll fluorescence, and the volume scattering function. Insert photograph shows a special copper shutter device for minimizing biofouling of the sensors. Photographs provided by Derek Manov.

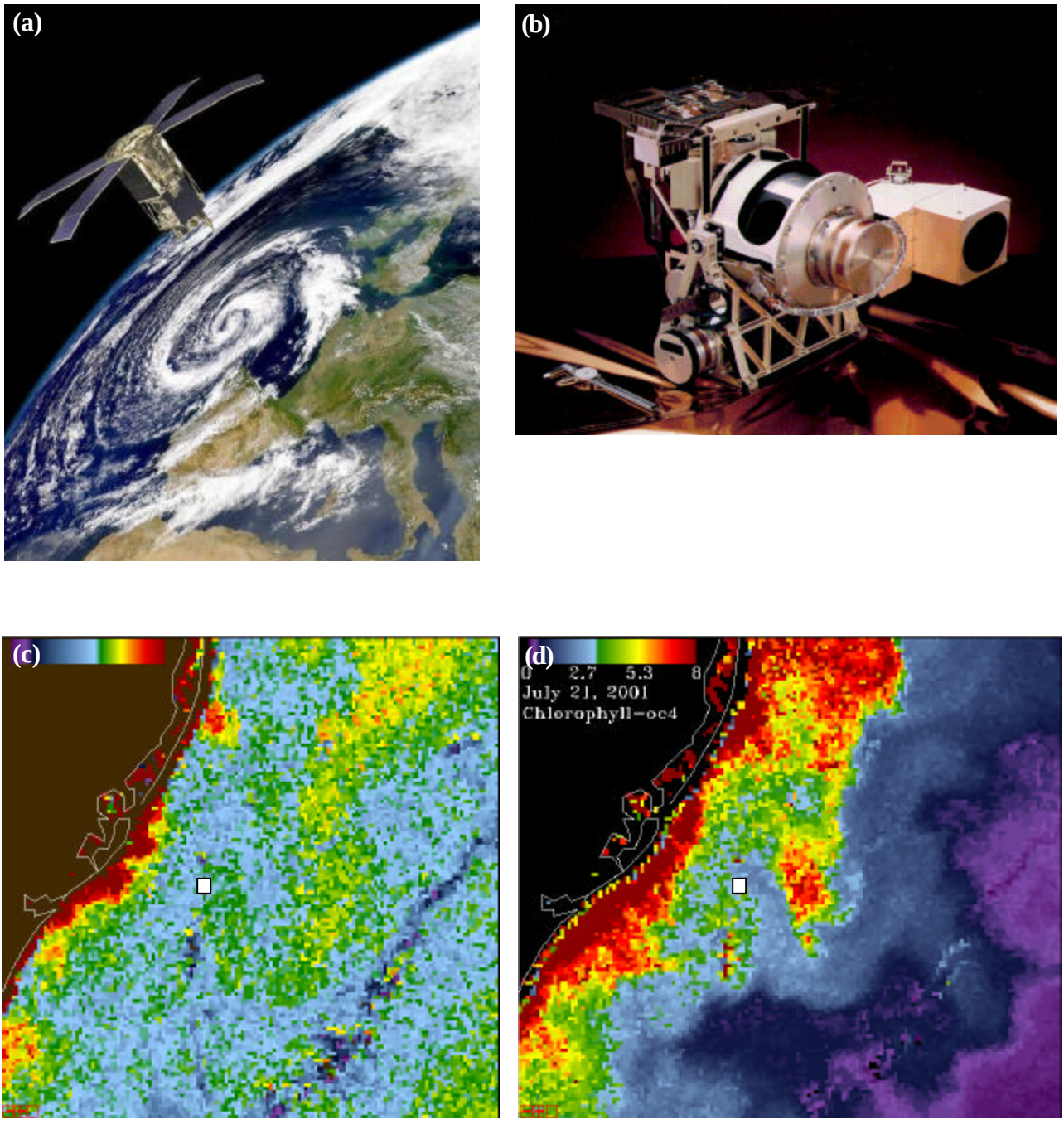

Fig. 3. (a) and (b) Photographs of the Sea-viewing Wide Field-of-view Sensor (SeaWiFS) for ocean color imaging at seven wavelengths. Photographs provided by NASA Goddard Space Flight Center. Example images of (c) remote sensing reflectance at 510 nm and (d) chlorophyll a concentration derived from SeaWiFS data at the LEO-15 site (white box) off the New Jersey coast. Images courtesy of Richard Gould.

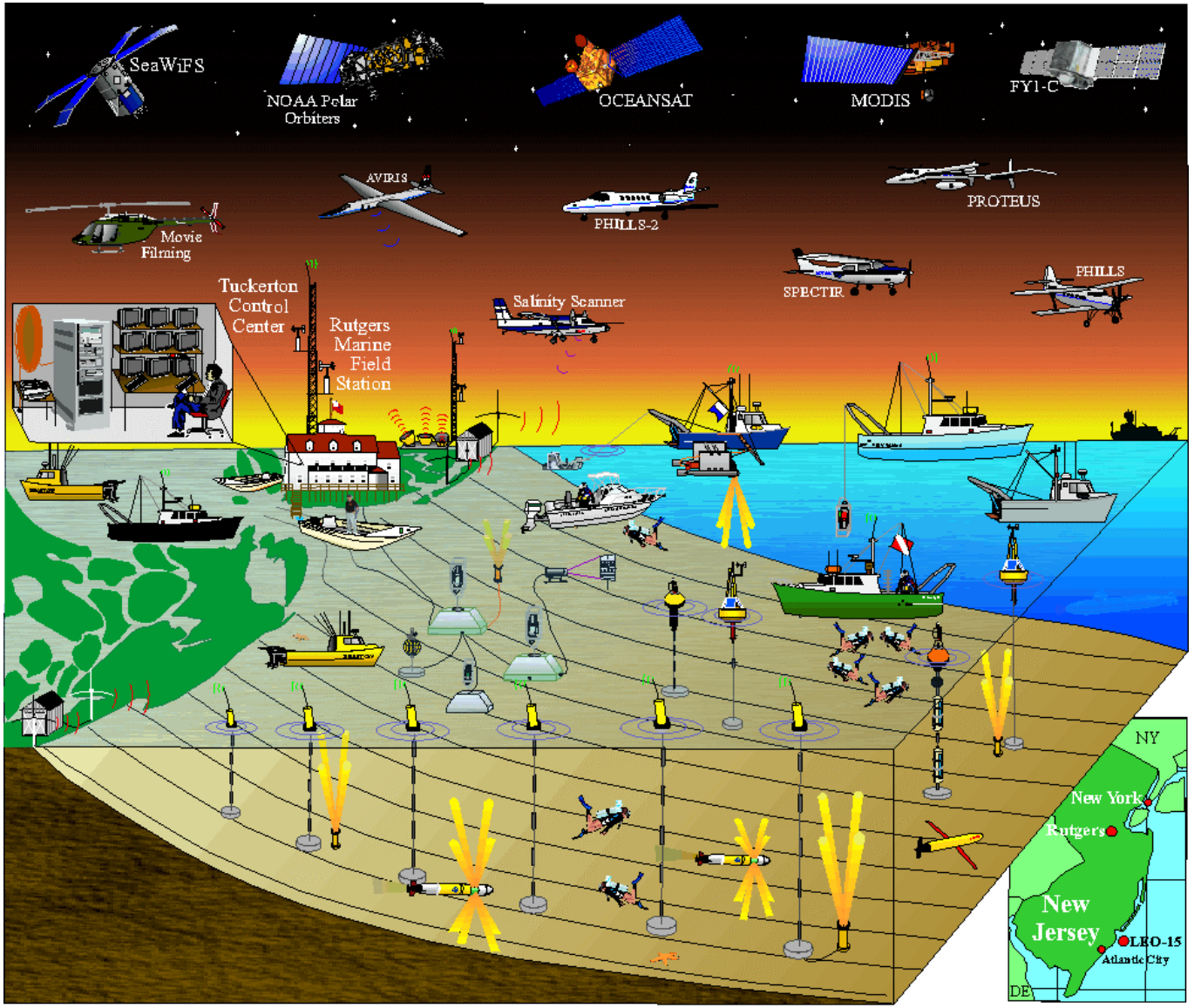

Fig. 4. Schematic diagram illustrating the various platforms used for the HyCODE experiments at the LEO-15 study site off the New Jersey coast in the summers of 2000 and 2001. Image provided by Scott Glenn.

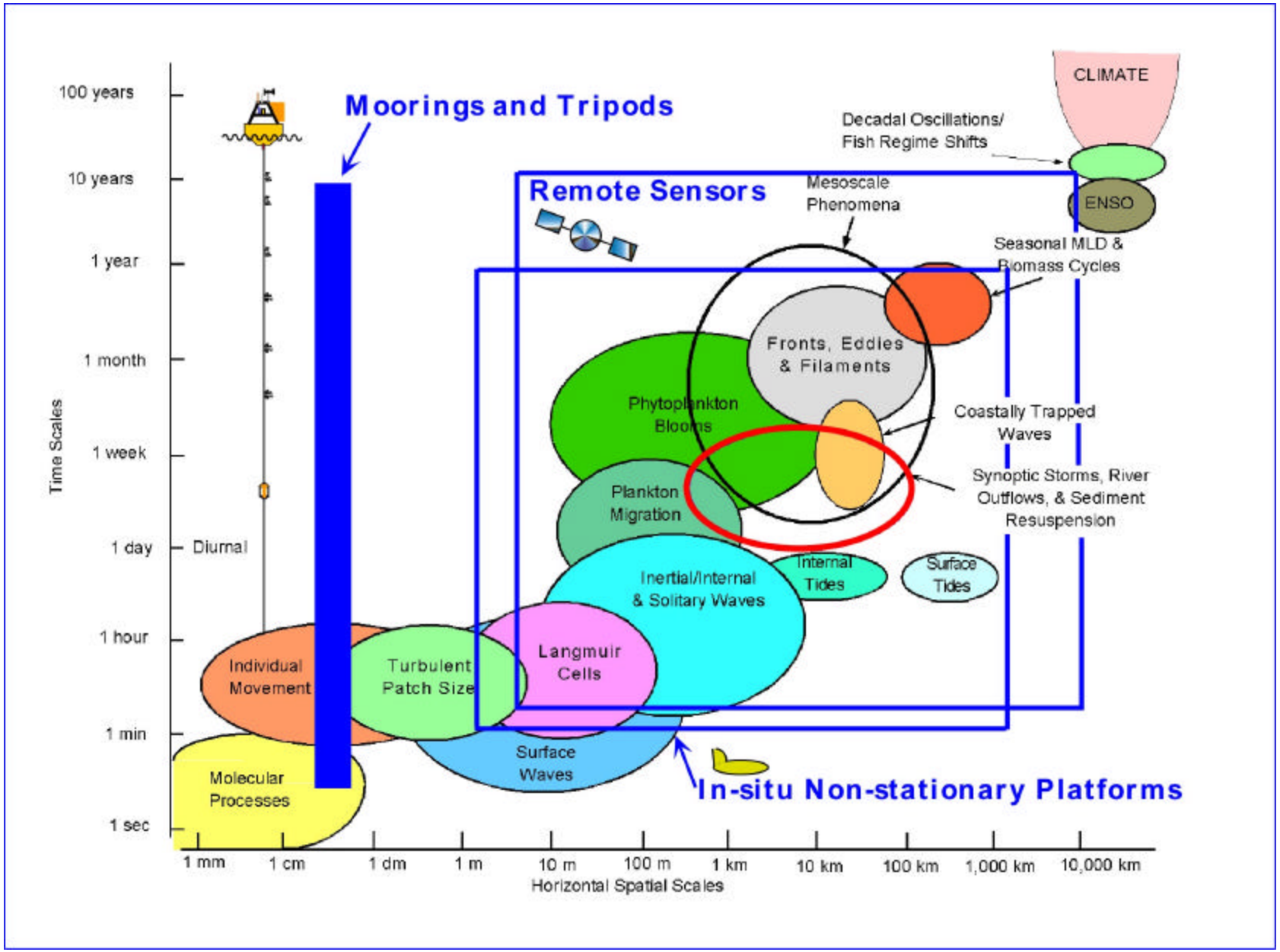

Fig. 5. Time-horizontal space diagram illustrating physical and biological processes overlain with sampling domains of various platforms (moorings, satellites, AUVs, etc.).

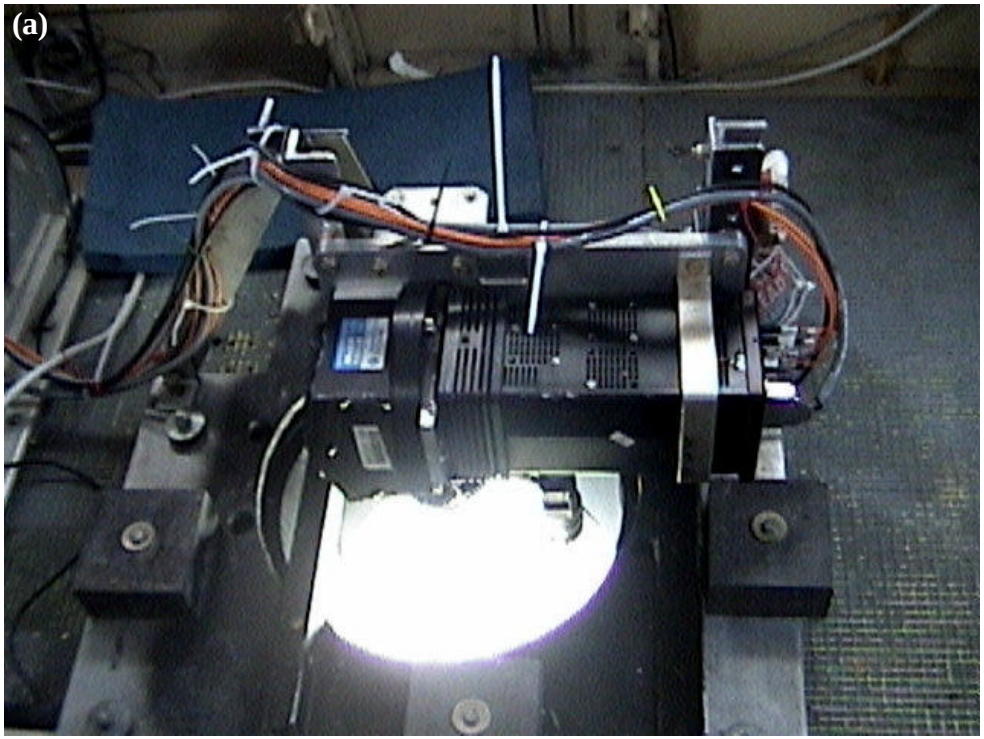

Fig. 6. (a) Photograph of the Ocean Portable Hyperspectral Imager for Low-Light Spectroscopy (PHILLS), a hyperspectral imaging spectrometer operating over the wavelength range 400 to 1000 nm with 1.7 nm spectral resolution. (b) PHILLS image taken at the LEO-15 site on July 22, 2000 (image stretched north-south). Image courtesy of Curtiss Davis.

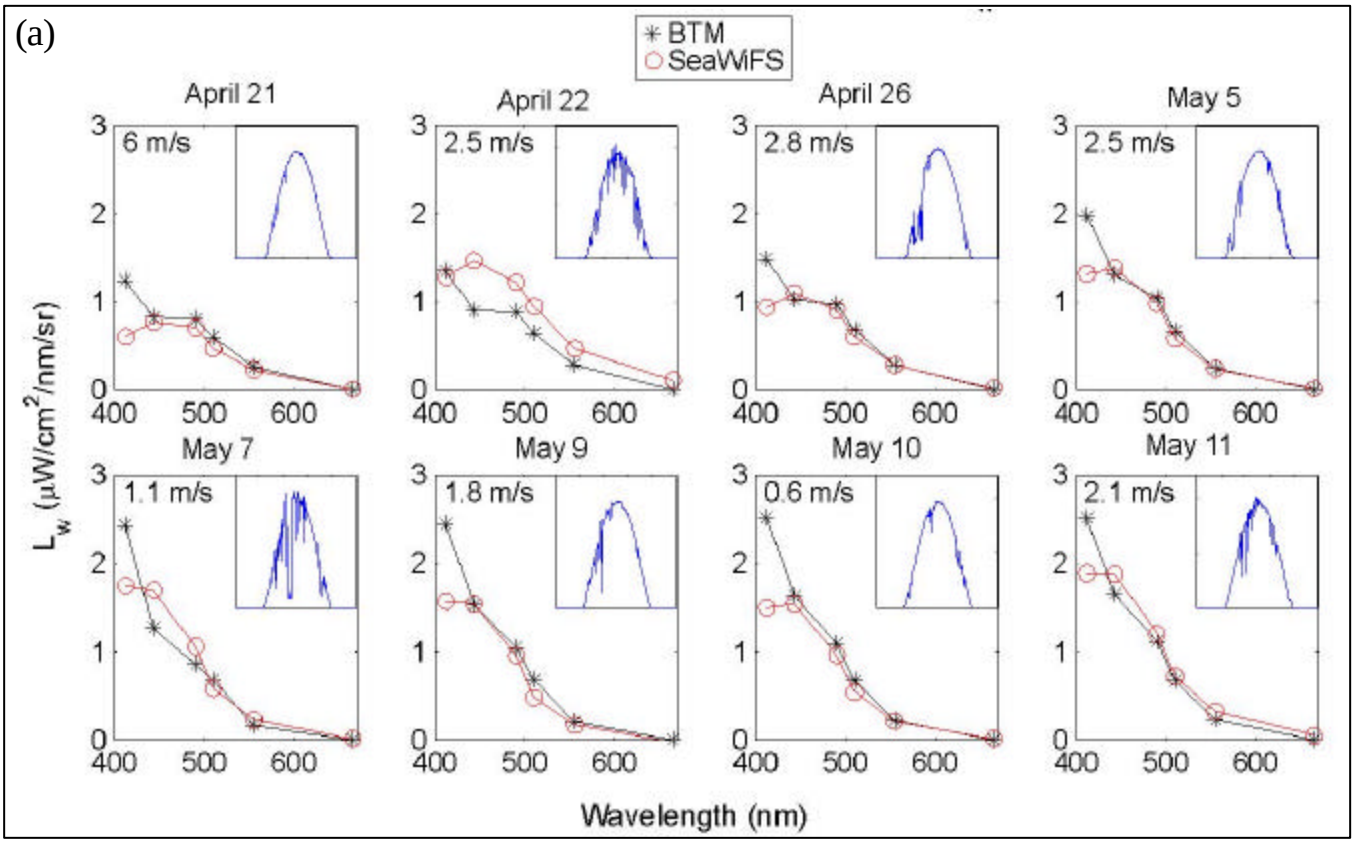

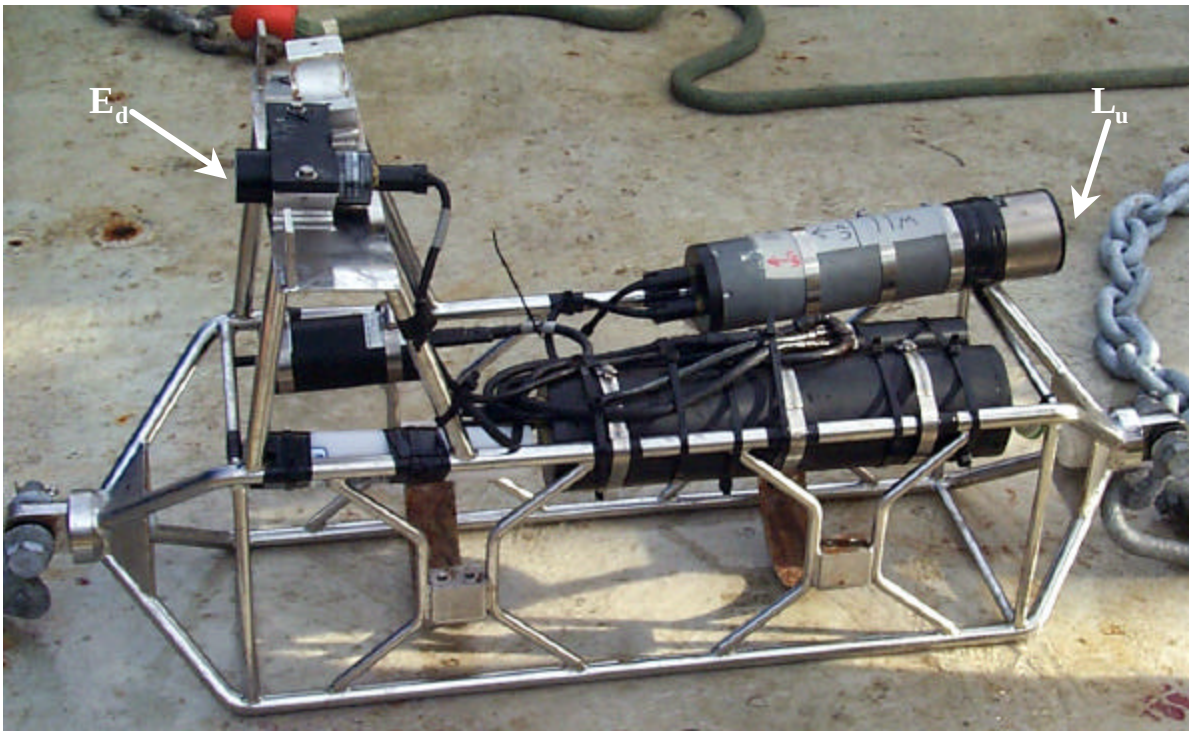

Fig. 7. (a) Spectral water-leaving radiance derived from Bermuda Testbed Mooring (BTM) radiometers and from the SeaWiFS ocean color satellite for eight days in 1999. Inserts show surface PAR time series to illustrate sky conditions. Daily average wind speeds are also indicated. (b) Photograph of the radiometric system deployed on the BTM. Radiometers are labeled.

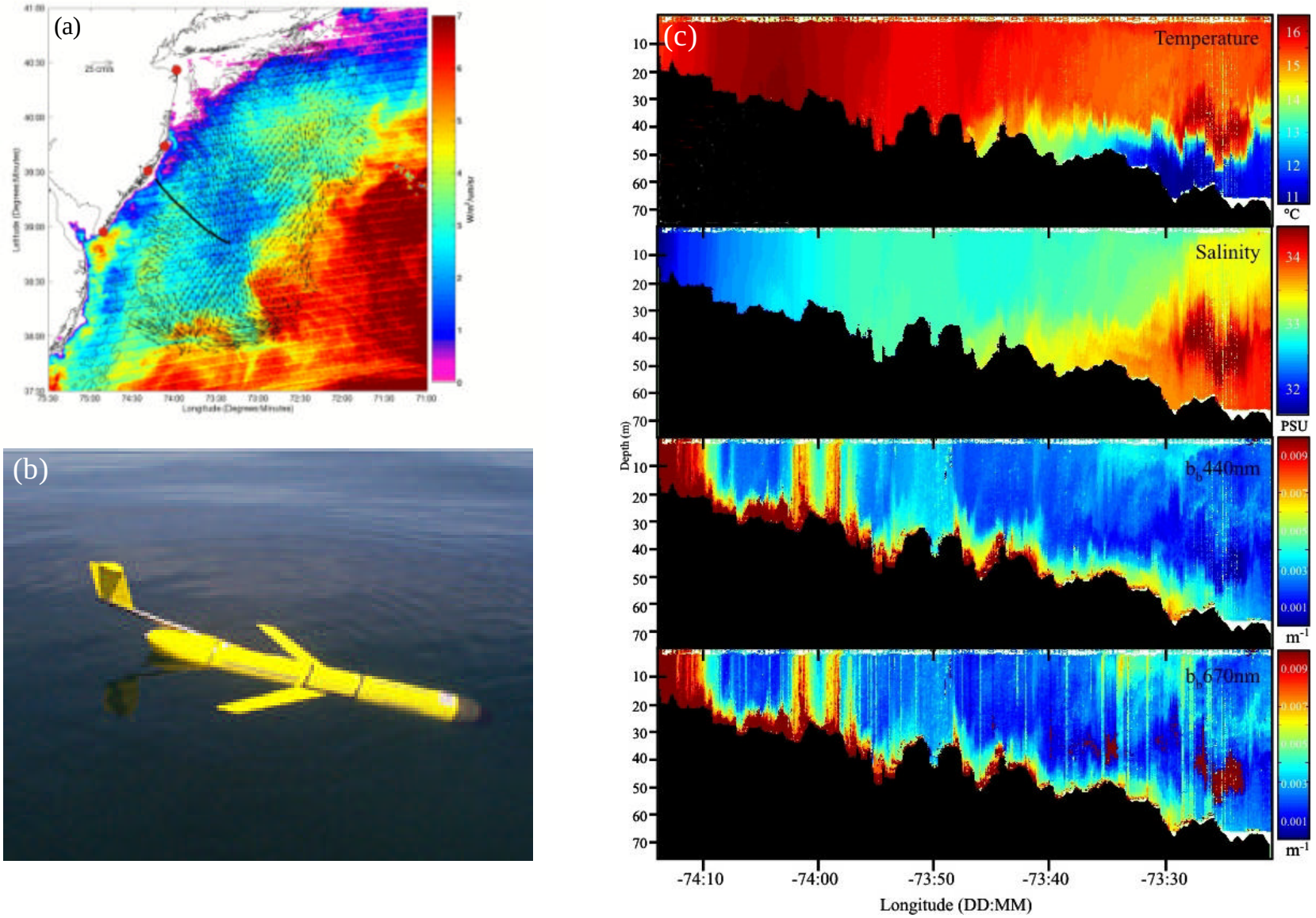

Fig. 8. (a) The dark, black line shows the six-day (October 28 to November 2, 2003), cross-shelf track of the Slocum Glider overlaid on the satellite-derived normalized water leaving radiance image at 443 nm from October 30, 2003. (b) Photograph of the Slocum glider. This particular glider is equipped with sensors to measure temperature, salinity, and optical properties. (c) Cross-shelf sections of temperature, salinity, and particulate backscatter at 440 and 670 nm measured by the Slocum glider (track shown in a). With permission from Oceanography Magazine, The Oceanography Society.

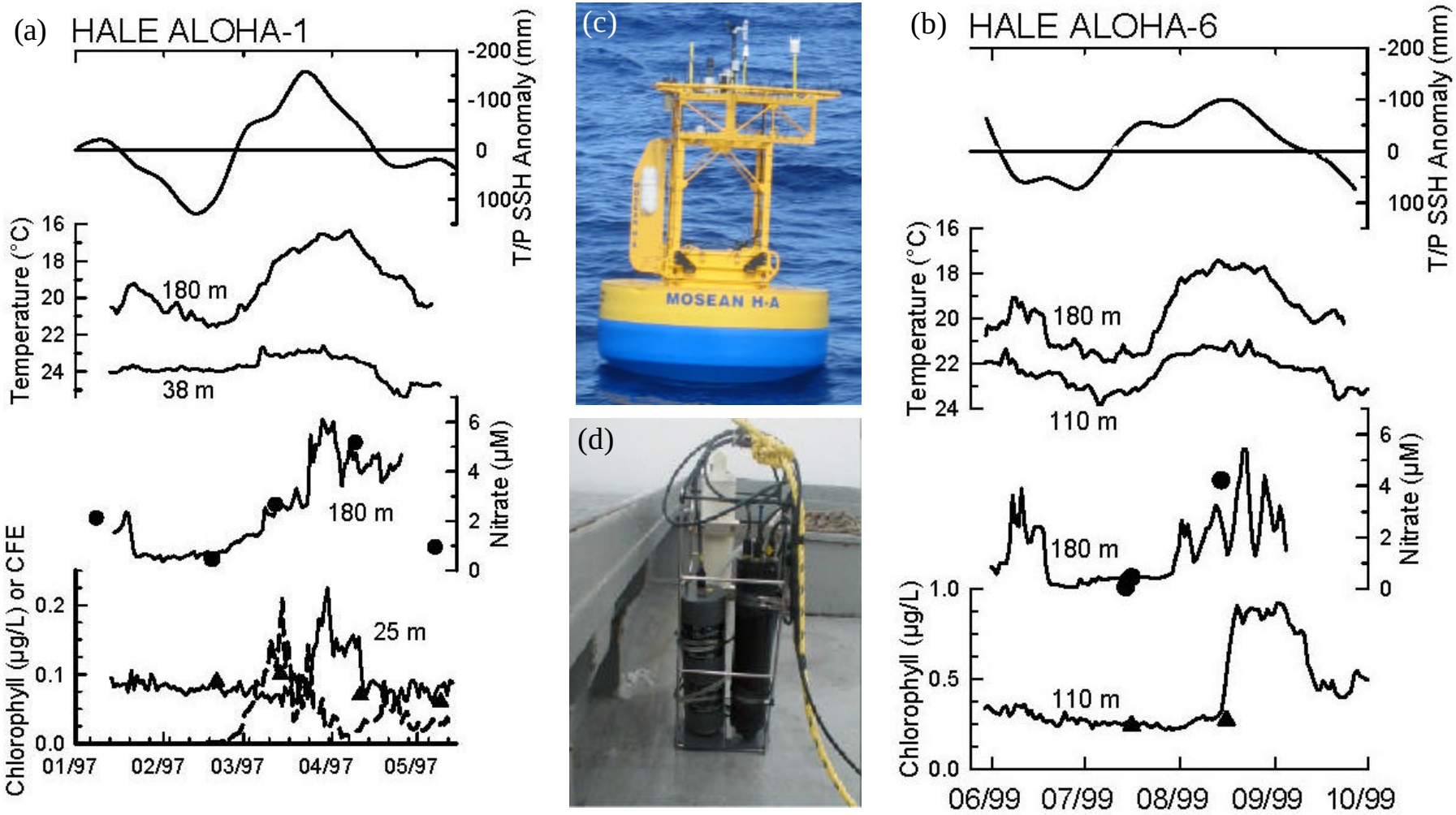

Fig. 9. (a) Tommy, fill in figure caption for a and b. Courtesy of Carole Sakamoto. (c) Photograph of the HALE-ALOHA buoy, as currently deployed, and (d) photograph of a newly developed chemical sensor, the In Situ Ultraviolet Spectrophotometer (ISUS), courtesy of Satlantic, Inc.

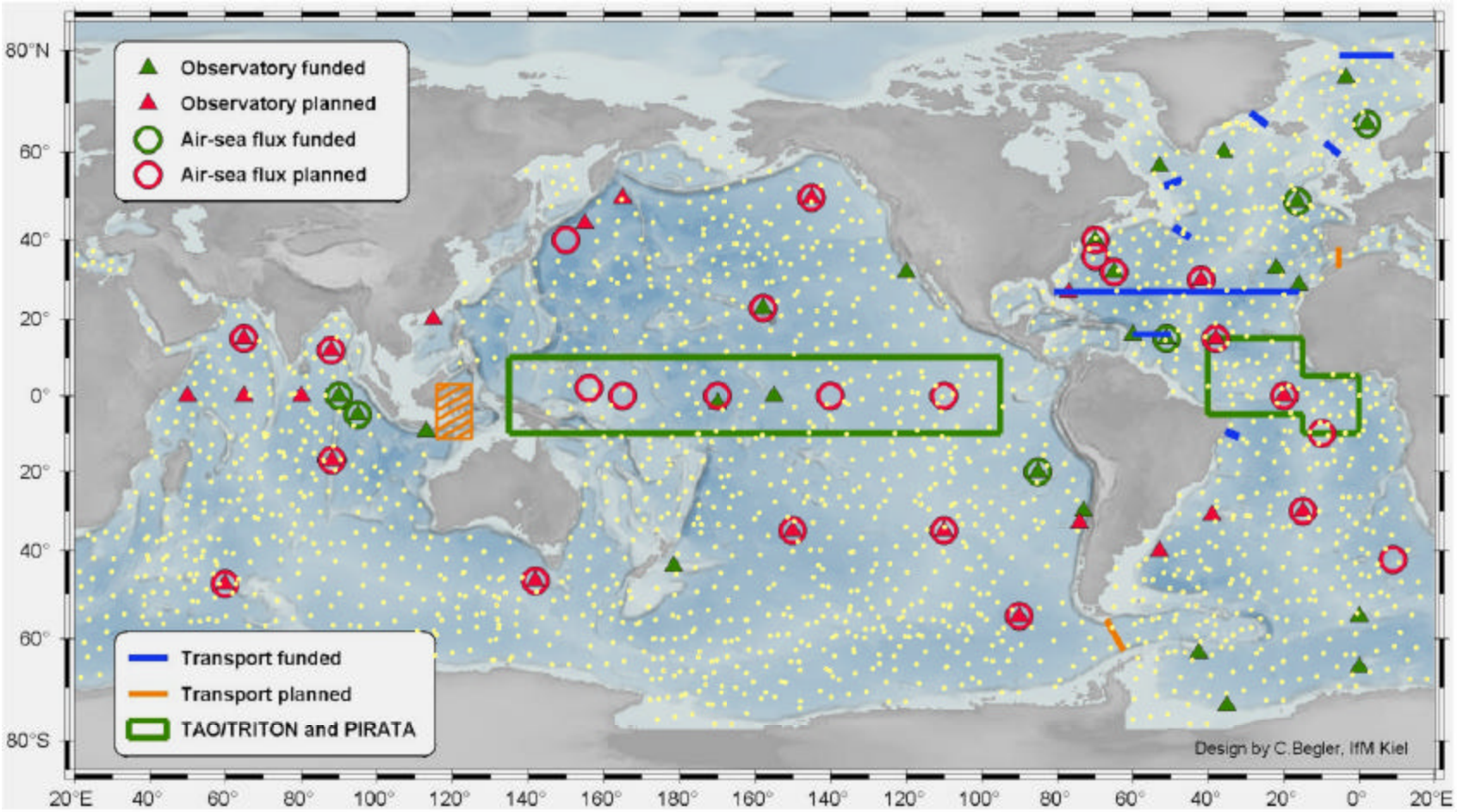

Fig. 10. Map of existing and planned time series platforms for the Global Ocean Observing System. Air-sea interaction stations are indicated by open circles, observatories by filled squares, and transport sections by rectangles (based on figure by Send et al., 2001) Superimposed on the map are white dots depicting planned global distribution of Argo profiling floats (based on figure by Roemmich et al., 2001).

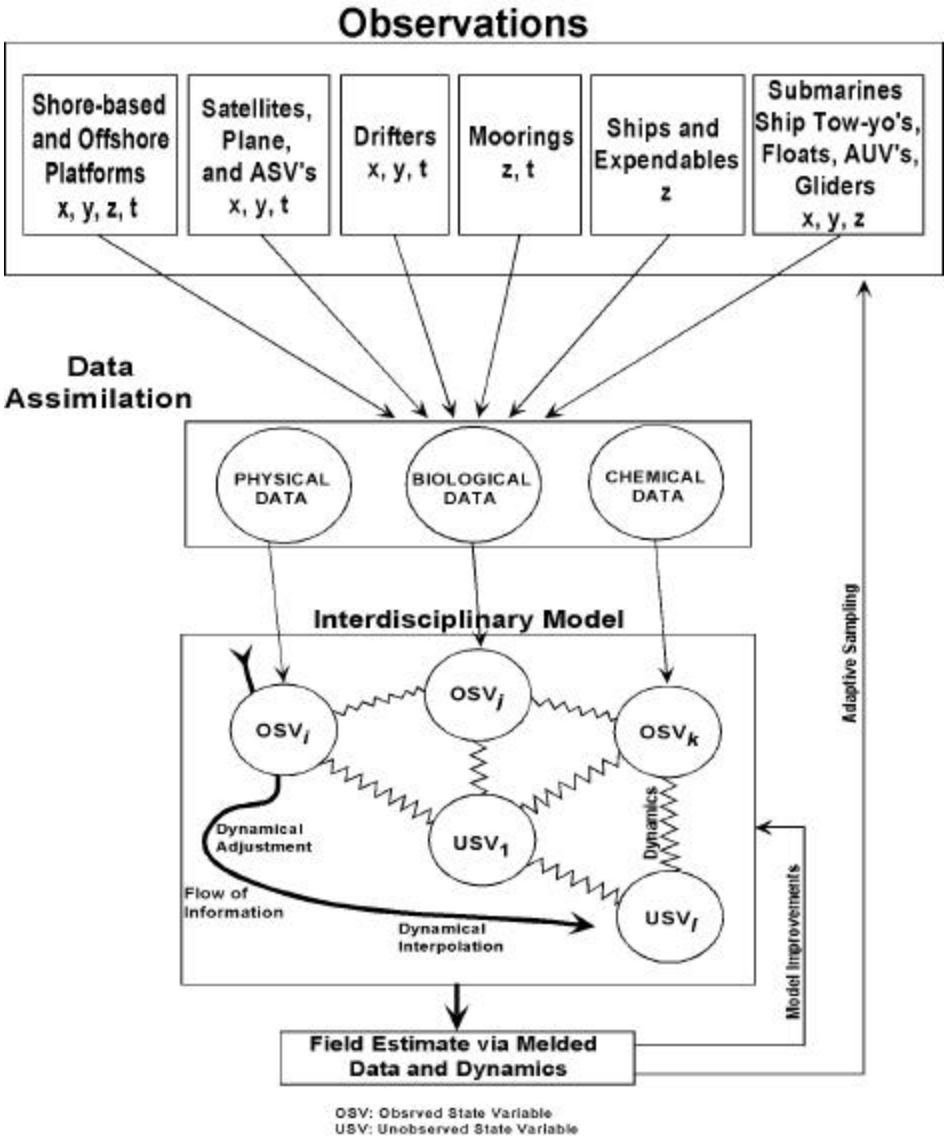

Fig. 11. Schematic illustrating the input of multi-disciplinary data into a data assimilation model along with feedbacks for model improvement and adaptive sampling. Lower portion of diagram is based on Fig. 3 of Dickey, 2003.